Detecting and characterizing mesoscale and submesoscale structures of Mediterranean water from joint seismic and hydrographic measurements in the Gulf of Cadiz

Elise Quentel, X. Carton, Marc-André M-A Gutscher, R. Hobbs

Detecting and characterizing mesoscale and submesoscale structures of Mediterranean water from joint seismic and hydrographic measurements in the Gulf of Cadiz

E. Quentel,[1,2] X. Carton,[1,3] M.-A. Gutscher,[1,2] and R. Hobbs[4]

Received 2 February 2010; accepted 18 February 2010; published 26 March 2010.

[1] Marine seismic and hydrographic data from the GO cruise in the Gulf of Cadiz acquired in April 2007 are analyzed to determine the physical nature and geometric characteristics of acoustic reflectors in the water column. Seismic data show strong reflectors near the surface, above Mediterranean water (MW) undercurrents, above a meddy, and within a submesoscale MW structure. These reflectors are associated with thermohaline layering. Wavelet analysis of seismic and hydrographic data (both in terms of reflectivity) shows strong signals with 12–48 m vertical wavelength scales. Hydrological data with its high vertical resolution, capture weaker signals with shorter wavelengths. At the edge of a meddy, lateral intrusions of fresher water are revealed by reflectors with 25–75 m thickness. Analyses of marine seismic data allow detection of submesoscale eddies that hydrographic sections identify only occasionally. **Citation:** Quentel, E., X. Carton, M.-A. Gutscher, and R. Hobbs (2010), Detecting and characterizing mesoscale and submesoscale structures of Mediterranean water from joint seismic and hydrographic measurements in the Gulf of Cadiz, *Geophys. Res. Lett.*, *37*, L06604, doi:10.1029/2010GL042766.

1. Introduction

[2] The first oceanographic structures to be observed using marine seismic reflection profiles were internal waves [*Gonella and Michon*, 1988]. More recently, oceanographic fronts in the northern Atlantic were studied and correlated to thermohaline structure on the basis of salinity and temperature measurements [*Holbrook et al.*, 2003; *Nandi et al.*, 2004]. Other scientists expanded the method to better image reflectors in the water column [*Holbrook and Fer*, 2005; *Biescas et al.*, 2008; *Krahmann et al.*, 2008; *Klaeschen et al.*, 2009; *Pinheiro et al.*, 2010]. This paper analyzes simultaneously acquired marine seismic and densely spaced physical oceanography data from the GO Cruise (HMS *Discovery* April/May 2007) in the Gulf of Cadiz [*Hobbs*, 2008]. Here sharp contrasts in thermohaline structure are present due to the Mediterranean waters. The objectives of this study are: to present a wavelet analysis of the characteristic length scales of seismic reflection and oceanographic structures, and to interpret the imaged structures in terms of mesoscale and submesoscale eddies, of homogeneous layers and of lateral intrusions.

2. Data Collection and Processing

[3] Warm and salty Mediterranean water (MW) flows out of the Mediterranean Sea at 150–200 m depth. Outflowing MW cascades down the continental slope and mixes with surrounding waters producing several undercurrents along the Iberian margin at depths of 400, 800 and 1200 m depths [*Madelain*, 1970; *Zenk*, 1975]. Canyons incising the continental slope destabilize these undercurrents and lead to the formation of mesoscale eddies (among which are anticyclones called Meddies [*Bower et al.*, 1995; *Bower*, 1997; *Serra and Ambar*, 2002]), and of submesoscale structures (small eddies and filaments) observed by oceanographic data [*Ambar et al.*, 2002]. However, until now no joint oceanographic-seismic experiment had ever provided a complete view of these structures.

[4] The GO cruise (17 April–14 May 2007) acquired synchronous and co-located seismic reflection and hydrographical data in the Gulf of Cadiz (www.dur.ac.uk/eu.go). To investigate the nature and characteristics of acoustic reflectors located between the warm, salty MW and neighboring water masses, three types of seismic sources were used. Here, only two "low-resolution" (LR) seismic profiles are presented. Acquisition parameters are: a 2320 cu in source (6 BOLT 1500L guns) (2× beams of 700, 300, 160 cu in guns) recorded by 2400 m long SERCEL streamer, towed at 8 m depth with 192 traces (12.5 m spacing). The expected vertical resolution was 15 m. The horizontal resolution of the continuous seismic profiles (10 m) is much finer than that of oceanographic data, which is typically 5–10 km. Seismic data processing includes bandpass filter between 4 and 8 Hz. Since the direct wave disturbs the signal at the surface layer, its removal is important. We used an eigenvector filter coupled with a low cut filter for direct wave removal. For more accurate removal, we used a novel application of an eigenvector filter, which linearly moves out traces based on previous work on multiple suppression [*Hardy and Hobbs*, 1991]. Noise reduction by time variant scaling is performed before stacking.

[5] Hydrographic sections along the Iberian margin were constructed using 45 XBT (eXpendable Bathy-Temperature probe) profiles acquired simultaneously while the seismic profiles were shot. A second vessel (R/V Poseidon) followed about 1.5 hours and 12 km behind the Discovery and performed CTD stations to complement the sections. 6 CTD profiles used in this study, cover the 0–2000 m depth range, while XBT reach a maximum depth of 1850 m. For XBT's, salinity was calculated from temperature via the density

[1]Université Européenne de Bretagne, Brest, France.
[2]Laboratoire Domaines Océaniques, IUEM, Technopole Brest Iroise, Plouzané, France.
[3]Laboratoire de Physique des Océans, UBO, Brest, France.
[4]Earth Sciences Department, Durham University, Durham, UK.

0094-8276/10/2010GL042766

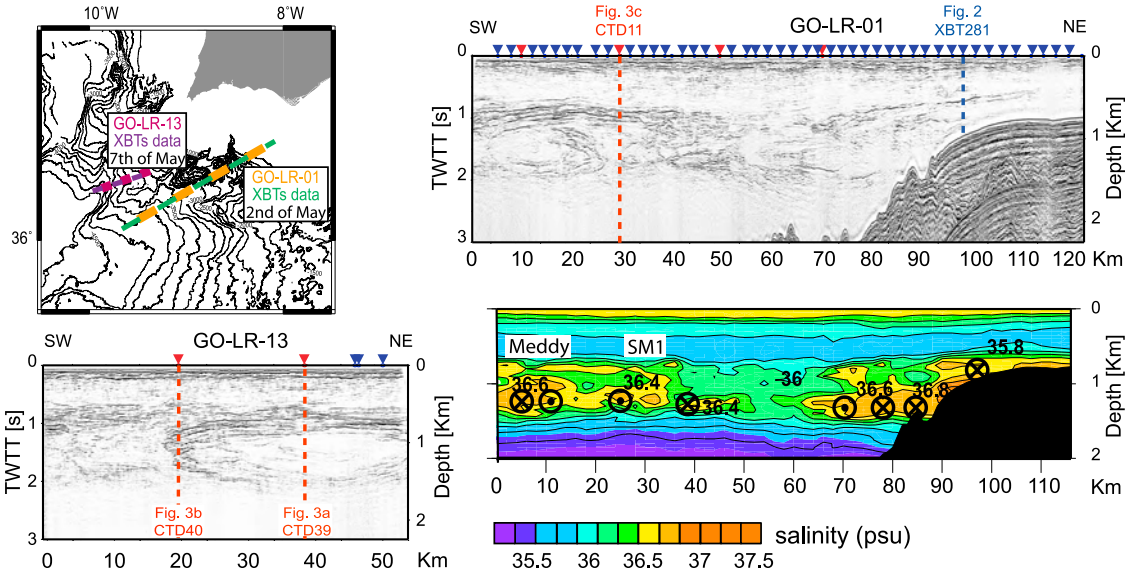

Figure 1. (top left) Position of seismic reflection and hydrographic cross-sections. (top right) Vertical sections of reflectivity and salinity LR-01 (scales are identical, but origins different). (bottom left) Vertical section of reflectivity of LR-13. Red triangles are CTDs and blue triangles are XBTs and XCTDs. (bottom right) Vertical section of salinity LR01. Velocity vectors (black bolt cross, velocities directed to the east; black bolt dot, velocities directed to the west) indicate an anticyclonic mesoscale eddy (a meddy), a cyclonic submesoscale eddy (SM1).

ratio method $r(z)$ [*Käse et al.*, 1996]. First, temperature and salinity data from 6 CTD's were divided into 3 subareas, and temperature and salinity differences (δT, δS) were calculated at each depth for each pair of CTD stations. The horizontal density ratio was then calculated as:

$$r(z) = \frac{\alpha\ \delta T}{\beta\ \delta S}$$

where α and β are the expansion coefficients for temperature and salinity. Then, for each XBT cast, a CTD reference station was first chosen with ($T_R(z)$, $S_R(z)$), and secondly, salinity S was derived from temperature T measured by the XBT via:

$$S = S_R + (T - T_R)\frac{\delta S}{\delta T} \text{ at each depth } z.$$

The accuracy of CTD temperature and salinity measurements is respectively ±0.001°C and ±0.001. The accuracy of XBT temperature and derived salinity is ±0.01°C and ±0.01.

2.1. Description of Seismic and Hydrographic Sections

[6] Figure 1 presents the two LR profiles: LR-01 (2nd of May) and LR-13 (7th of May). Salinity sections could be achieved only for LR-01, which sampled the MW undercurrents on the continental slope and offshore. On LR-01, seismic reflectors are observed in the near subsurface, and between 800 m and 2000 m depths. Several flow structures can be identified from the seismic reflection cross-sections:

[7] 1. The MW undercurrents on the continental slope, or their extrusion, located between km 60 and 110, with stronger reflectors between 500 and 800 m depths and weaker reflectors between 1400 and 1600 m depths. They extend relatively far offshore from the continental slope (30 km).

[8] 2. A lens-like body located between km 0 and 25, with a size and shape typical of a Meddy, based on prior observations and model predictions [*Serra et al.*, 2005; *Ambar et al.*, 2008]. It shows the strongest reflections at its upper boundary (between 700 and 1000 m depths) and somewhat weaker reflections at its base (depths of 1300–1400 m). In fact, this meddy extends much farther westward (and to the SW), as shown by section LR-13; LR-13 provides a diameter of at least 35 km for this meddy and images finer details at the edge of the meddy, with vertically stacked reflectors.

[9] 3. Between these two mesoscale structures, smaller structures are observed on section LR-01. An acoustically transparent structure with strong reflectors at its top (near 700–800 m depths) is present near km 30 of the LR-01 section, with about 10 km diameter, called submesoscale structure 1 (SM1) hereafter.

[10] The LR-01 hydrological section provides complementary information:

[11] 1. The MW undercurrents are well characterized by two distinct salinity maxima in the vertical dimension: the first (36.6 psu) lies near 800 m depth, while the second (36.8 psu) lies near 1200 m depth. High salinities (36.4 psu) extend far offshore of the continental slope (again at 30 km). These salinities contrast sharply with the surrounding Atlantic waters (which have S = 35.5–35.8 psu).

[12] 2. The meddy is well characterized by salinities of about 36.4 psu over a horizontal distance of 15 km.

[13] 3. The small scale structures, between the meddy and the undercurrents, are a fragment of high salinity waters with two maxima, at 800 and 1200 m depths, between km 20 and 30, at the location of SM1.

[14] To characterize the mesoscale and submesoscale structures, geostrophic velocities were calculated from density for XBT data, and the main velocity directions were

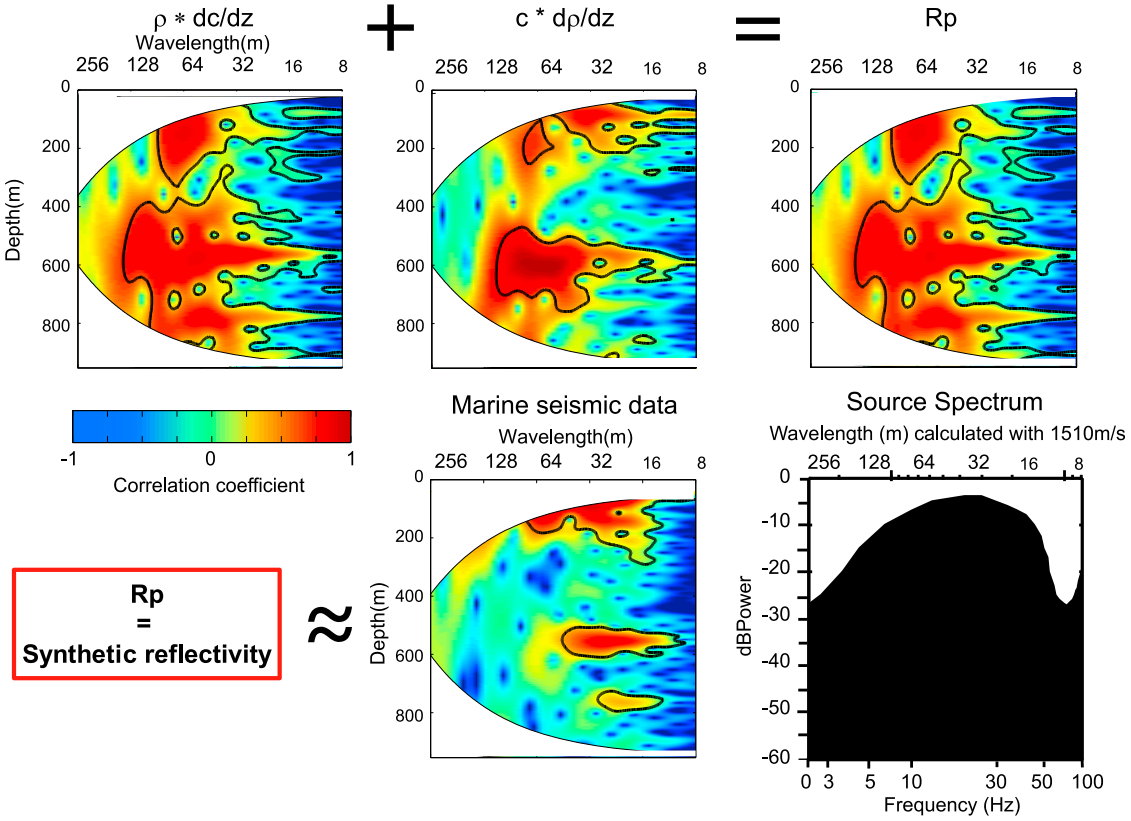

Figure 2. Wavelet analysis of real and synthetic reflectivity profiles through the MW undercurrents on the continental shelf. (top) Combination of vertical gradients of density and of sound speed (from hydrographic measurements) to provide synthetic reflectivity. (bottom) Real seismic reflectivity from adjacent traces stacked. Source spectrum of LR profiles. Wavelengths are calculated from frequencies by a sound speed in the water column of 1510 m s^{-1}. Frequencies are defined by the logarithm and correspond to a wavelength period in meters. The thick black contour designates the 5% significance level against red noise and the cone of influence (COI) where edge effects might distort the picture is shown as a lighter shade. Scale defined to blue (−1) from red (1) is the normalized correlation coefficient.

superimposed on the salinity cross-section (Figure 1). The anticyclonic body between 0 and 10 km is a Meddy. Between 25 and 50 km, SM1 appears as a cyclonic eddy. Between 65 and 80 km, a cyclonic structure is related to the large extrusion of salty water at 1200–1300 m depth. The shallower velocity signal on the slope is related to the MW undercurrents. The velocity normal to the section changes sign at 1000 m depth and near 80–90 km. We interpret this reversal as a meander of the MW undercurrents, cut obliquely by section LR-01, which is nearly parallel to the continental slope here.

2.2. Wavelet Analysis of Vertical Seismic and Hydrographic Profiles

2.2.1 Calculation of Synthetic Reflectivity Data

[15] Wavelet analysis is used to identify the size and wavelength of mesoscale and submesoscale structures. The analysis is a Continuous Wavelet Analysis modified from *Grinsted et al.* [2004] using a Morlet wavelet with parameters of vertical distance and vertical wavelength defined as:

$$\psi_0(\eta) = \pi^{-\frac{1}{4}} e^{i\omega_0\eta} e^{-\frac{1}{2}\eta^2}$$

where ω_0 is dimensionless wavenumber and η is dimensionless distance (on the entire column). A value of $\omega_0 = 6$ was chosen to provide a good balance between distance and wavelength determination. The continuous Wavelet Transform (CWT) can be seen as a consecutive series of band-pass filters applied to the depth series where the wavelet scale is linearly related to the characteristic period of the filter. The CWT has edge artifacts because the wavelet is not completely localized in depth.

[16] Synthetic gradients of acoustic impendance data were calculated from hydrographic data for comparison with the real seismic data (adjacent traces stacked). Reflections across the water column are induced by acoustic impedance contrasts due to strong gradients of temperature and salinity between water masses. Acoustic impedance is defined as:

$$I = \rho c$$

where ρ is density and c is sound speed.

[17] The synthetic gradient of acoustic impedance is calculated from hydrography as:

$$Zs = \frac{dI}{dz} = c\frac{d\rho}{dz} + \rho\frac{dc}{dz}$$

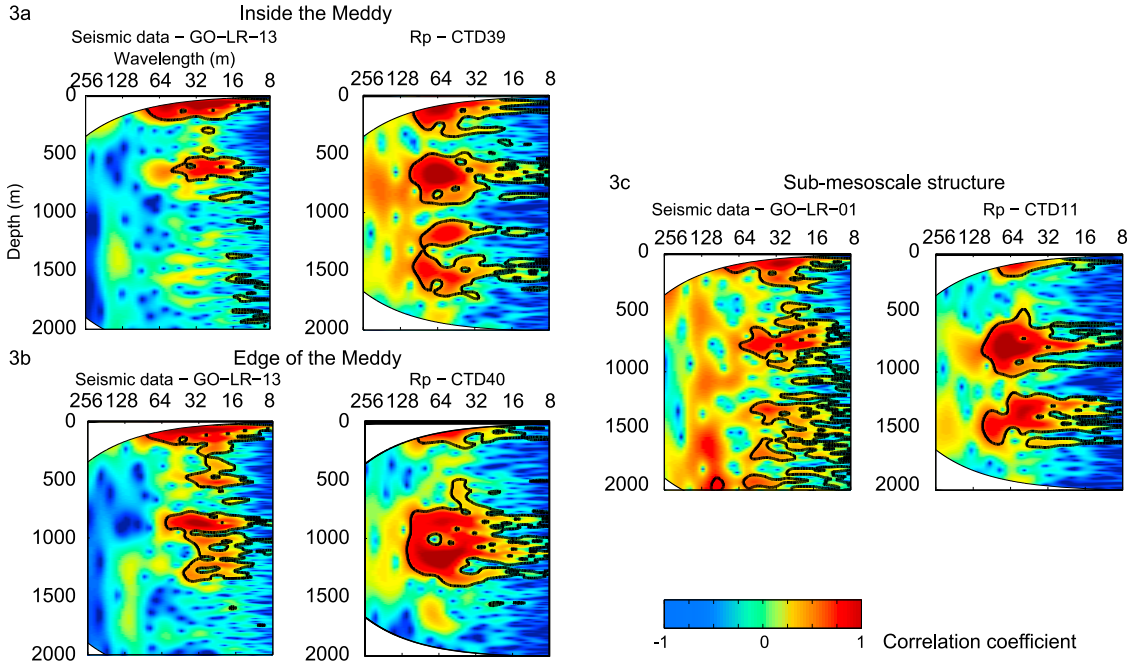

Figure 3. Wavelet analysis (a) in a Meddy and (b) near a Meddy and (3c) in the Submesoscale structure SM1. The left-hand columns of plots are real seismic data. The right-hand columns are synthetic reflectivity data. Frequencies as in Figure 2.

[18] The reflectivity coefficient is then calculated from hydrology as:

$$Rp = \frac{1}{c}\frac{dc}{dz} + \frac{1}{\rho}\frac{d\rho}{dz} = \frac{1}{\rho c}\frac{d}{dz}(\rho c)$$

and the filter applied on seismic data is implemented on this reflectivity coefficient. The filter is a band-pass between 4 Hz and 8 Hz. The seismic data and this coefficient of reflectivity can now be compared. Density and sound speed are calculated from temperature and pressure of CTD data [*Käse et al.*, 1996; *Ruddick et al.*, 2009].

2.2.2. Across the MW Undercurrents

[19] Figure 2 shows the vertical wavelet analysis through the upper MW undercurrent on the continental slope near Portimo Canyon (LR-01 section, see Figure 1 for location). Both real and synthetic data show strong reflectivity in the upper ocean layers and above the MW undercurrents. The wavelengths of the signal found in both data sets are 8–64 m. Both the density and the sound speed gradient show features in these depth ranges and at these wavelengths. Nevertheless, differences can be observed between real and synthetic seismic data:

[20] 1. Synthetic data show stronger reflectivity than the real seismic data (the real signal is less spread out vertically). This may be related to loss of acoustic energy in the water column.

[21] 2. Synthetic data also display shorter vertical wavelengths (due to the higher vertical resolution of CTD measurements), and longer wavelengths (which correspond to taller thermohaline gradients in the transition zone between Atlantic and Mediterranean waters).

[22] 3. The density and sound speed components show maxima at different depths: the sound speed gradient is stronger in the near subsurface and below 800 m depth; the density gradient is maximum near 600 m depth.

2.2.3. Across a Meddy and at its Edge

[23] The real seismic reflectivity profile, across the meddy center, shows reflectors in the near subsurface and between 600 and 800 m depths (the upper part of the meddy), with dominant wavelengths between 16 and 64 m (see Figure 3a). The meddy core is transparent and weak reflectivity is observed below the meddy. The synthetic reflectivity, calculated from CTD casts on section LR-13 (which have a better precision than that of XBT data), shows strong reflectivity at the same depths. But it also shows reflectivity below the meddy, with thickness of about 32 to 64 m. Both above and below the meddy, the strong reflectivity is associated with thermohaline layering. At the meddy edge, real seismic data show continuous reflectivity between 800 and 1300 m, but also near the surface (see Figure 3b). Synthetic data are intense at the same depths, but with a larger range of wavelengths at the meddy center (8–80 m instead of 16–64 m). This strong reflectivity is interpreted as the result of lateral intrusions of external water into the meddy, leading to interleaving (vertical alternance of saltier and fresher water layers). Indeed, *Ruddick and Hebert* [1988] identified the origin of fine-scale structures at the edge of meddy "Sharon" as lateral intrusions of Atlantic water associated with salt fingering. They performed temperature gradient autospectra in this intrusive zone and determined vertical scale for these structures of 25 to 75 m. These characteristic wavelengths are identical to those found with seismic reflectivity.

2.2.4. In the Submesoscale Structure

[24] One CTD cast (CTD11) across submesoscale structure SM1 is now analyzed in terms of coefficient of reflectivity, and compared to real reflectivity (Figure 3c); it shows differences between real and synthetic data. Real seismic data present a nearly continuous series of reflectors from the surface to 2000 m depth with characteristic wavelengths of 16–

64 m, the 400–600 and 800–1200 m intervals being more transparent. Synthetic reflectivity computed from CTD11 identifies strong reflectors near the surface, above and below the MW structure with dominant wavelengths between 16 and 80 m. It clearly shows a transparent region between 300 and 600 m and between 800 and 1200 m. The signal is clearly stronger and more coherent vertically in the synthetic signal. We interpret this difference by the tendency of synthetic data to emphasize the strongest thermohaline contrast.

3. Conclusion

[25] Seismic reflection and hydrographic cross-sections were interpreted in terms of mesoscale and submesoscale structures, while vertical wavelet analysis provided the characteristic scales of these structures. On the continental slope, strong reflectors were observed above the shallow vein of MW. A meddy was clearly identified in seismic and hydrographic data, via strong reflectors at its top, and vertically more continuous reflectors at its edge. The reflectors above the meddy correspond to the boundaries of homogeneous layers. The lateral reflectors have the same vertical wavelength as thermohaline intrusions and are likely to result from such intrusions. A submesoscale feature observed along the LR-01 section was characterized by a vertically continuous array of reflectors in the real seismic date, whereas the synthetic data concentrated again on the strongest vertical thermohaline gradients.

[26] The horizontal resolution of seismic data is much finer (12.5 m) than that of hydrographic data (5–10 km). Thus, seismic measurements can detect and characterize deep submesoscale eddies more efficiently, more accurately and more rapidly than hydrographic sections. Furthermore, altimetric measurements of sea-level anomaly are not accurate near the coast and thus, cannot identify submesoscale eddies. Therefore, marine seismic measurements, which can rapidly cover the Portimão Canyon - Cape Saint Vincent region, are probably the best method for monitoring the formation and flux of mesoscale and submesoscale eddies off Iberia.

[27] **Acknowledgments.** The GO project was funded by the 6th EU Framework for research and development. The authors of the present paper wish to thank the captain and crew of the HMS *Discovery* and GO partners, particularly Dirk Klaeschen and Cord Pappenberg from Ifm-GEOMAR who performed the processing of the seismic profiles used.

References

Ambar, I., N. Serra, M. Brogueira, G. Cabeadas, F. Abrantes, P. Freitas, C. Gonalves, and N. Gonzalez (2002), Physical, chemical and sedimentological aspects of the mediterranean outflow off Iberia, *Deep Sea Res., Part II*, *49*, 4163–4177.

Ambar, I., N. Serra, F. Neves, and T. Ferreira (2008), Observations of the Mediterranean undercurrent and eddies in the Gulf of Cadiz during 2001, *J. Mar. Syst.*, *71*(1–2), 195–220, doi:10.1016/j.jmarsys.2007.07.003.

Biescas, B., V. Sallars, J. L. Pelegr, F. Machn, R. Carbonell, G. Buffett, J. J. Daobeitia, and A. Calahorrano (2008), Imaging meddy finestructure using multichannel seismic reflection data, *Geophys. Res. Lett.*, *35*, L11609, doi:10.1029/2008GL033971.

Bower, A. S. (1997), Lagrangian observations of meddy formation during a Mediterranean undercurrent seeding experiment, *J. Phys. Oceanogr.*, *27*, 2545–2575.

Bower, A. S., L. Armi, and I. Ambar (1995), Direct evidence of meddy formation off the southwestern coast of Portugal, *Deep Sea Res., Part 1*, *42*(9), 1621–1630.

Gonella, J., and D. Michon (1988), Ondes internes profondes révélées par sismique réflexion au sein des masses d'eau en atlantique-est, *C. R. Acad. Sci., Ser. II*, *306*, 781–787.

Grinsted, A., J. C. Moore, and S. Jevrejeva (2004), Application of the cross wavelet transform and wavelet coherence to geophysical time series, *Nonlinear Processes Geophys.*, *11*(5/6), 561–566.

Hardy, R., and R. Hobbs (1991), Multiple suppression in deep water, in *Continental Lithosphere: Deep Seismic Reflections*, *Geodyn. Ser.*, vol. 22, edited by R. Meissner et al., pp. 383–390, AGU, Washington, D. C.

Hobbs, R. (2008), Rrs discovery d318a & d318b, cruise report, geophysical oceanography, *Tech. Rep. 15603*, Dep. of Earth Sci., Univ. of Durham, Durham, U. K.

Holbrook, W. S., and I. Fer (2005), Ocean internal wave spectra inferred from seismic reflection transects, *Geophys. Res. Lett.*, *32*, L15604, doi:10.1029/2005GL023733.

Holbrook, W. S., P. Paramo, S. Pearse, and R. W. Schmitt (2003), Thermohaline fine structure in an oceanographic front from seismic reflection profiling, *Science*, *301*(5634), 821–824.

Käse, R. H., H. H. Hinrichsen, and T. B. Sanford (1996), Inferring density from temperature via a density-ratio relation, *J. Atmos. Oceanic Technol.*, *13*(6), 1202–1208, doi:10.1175/1520−0426(1996)013<1202:IDFTVA>2.0.CO;2.

Klaeschen, D., R. W. Hobbs, G. Krahmann, C. Papenberg, and E. Vsemirnova (2009), Estimating movement of reflectors in the water column using seismic oceanography, *Geophys. Res. Lett.*, *36*, L00D03, doi:10.1029/2009GL038973.

Krahmann, G., P. Brandt, D. Klaeschen, and T. Reston (2008), Mid-depth internal wave energy off the Iberian peninsula estimated from seismic reflection data, *J. Geophys. Res.*, *113*, C12016, doi:10.1029/2007JC004678.

Madelain, F. (1970), Influence de la topographie du fond sur l'écoulement méditerranéen entre le détroit de gibraltar et le cap saint-vincent, *Cahiers Océanogr.*, *22*, 43–61.

Nandi, P., W. S. Holbrook, S. Pearse, P. Paramo, and R. W. Schmitt (2004), Seismic reflection imaging of water mass boundaries in the Norwegian Sea, *Geophys. Res. Lett.*, *31*, L23311, doi:10.1029/2004GL021325.

Pinheiro, L. M., H. Song, B. Ruddick, J. Dubert, I. Ambar, K. Mustafa, and R. Bezerra (2010), Detailed 2-D imaging of the mediterranean outflow and meddies off west Iberia from multichannel seismic data, *J. Mar. Syst.*, *79*(1–2), 89–100, doi:10.1016/j.jmarsys.2009.07.004.

Ruddick, B., and D. Hebert (1988), The mixing of meddy "sharon", in *Small-Scale Turbulence and Mixing in the Ocean*, edited by J. C. J. Nihoul and B. M. Jamart, pp. 249–262, Elsevier, New York.

Ruddick, B., H. B. Song, C. Z. Dong, and L. Pinheiro (2009), Water column seismic images as maps of temperature gradient, *Oceanography*, *22*(1), 192–205.

Serra, N., and I. Ambar (2002), Eddy generation in the Mediterranean undercurrent, *Deep Sea Res., Part II, 49*, 4225–4243.

Serra, N., I. Ambar, and R. H. Kse (2005), Observations and numerical modelling of the Mediterranean outflow splitting and eddy generation, *Deep Sea Res., Part II*, *52*, 383–408.

Zenk, W. (1975), Some current and temperature observations in the Mediterranean outflow west of Gibraltar: A data report, *Meteor Forschungsergeb., Reihe A*, *15*, 20–48.

X. Carton, Laboratoire de Physique des Océans, UBO, 6 Avenue Le Gorgeu, 29200 Brest, France.

M.-A. Gutscher and E. Quentel, Laboratoire Domaines Océaniques, IUEM, Technopole Brest Iroise, 29280 Plouzané, France. (quentel@univ-brest.fr; elisequentel@gmail.com)

R. Hobbs, Earth Sciences Department, Durham University, Durham DH1 3HP, UK.